Zhu S, Shen WA and Xu YL (2012) Linear electromagnetic devices for vibration damping and energy harvesting: modeling and testing. *Engineering Structures*. 34: 198-212.

# Linear Electromagnetic Devices for Vibration Damping and Energy Harvesting: Modeling and Testing

Songye Zhu[1,*], Wen-ai Shen[1] and You-lin Xu[1]

[1] Department of Civil and Structural Engineering, The Hong Kong Polytechnic University, Hung Hom, Kowloon, Hong Kong

[*] Corresponding author: ceszhu@polyu.edu.hk

## ABSTRACT:

Over the past decades, the research on structural vibration control has mainly focused on 'energy dissipation' strategy using various dampers for hazard mitigation. This paper proposes a novel application of linear motion electromagnetic (EM) devices, termed linear EM dampers in this paper, for both vibration damping and energy harvesting. The kinetic energy caused by earthquakes, wind or traffic loads is not only dissipated by EM dampers, but also stored by energy-harvesting electric circuits connected to EM dampers. The green and regenerative energy output may provide an alternative power supply to portable and wireless devices at remote sites. This paper presents a theoretical and experimental study of linear EM dampers connected with four representative circuits. The dynamic characteristics of linear EM dampers, including parasitic damping, EM damping, energy conversion efficiency and effective output power, are modeled and discussed systematically in each case. The modeling is further verified by a series of dynamic testing of a small-scale linear EM damper, which is cyclically tested on a MTS machine at different frequencies and amplitudes. A good match between the modeling and testing results clearly demonstrates that the described model can predict the performance of the linear EM damper and energy harvesting circuit very well. The promises and challenges of using EM dampers in future civil infrastructure for both vibration damping and energy harvesting are discussed based on the outcome of this study.

**KEYWORDS:** electromagnetic damper, vibration control, energy harvesting, energy conversion efficiency

## 1. Introduction

Structural control and health monitoring, as two key components in smart structure technology, have seen significant progress in the past three decades. Structural control refers to the means of protecting primary structural system against dramatic vibrations and possible damages induced by traffics, wind, waves and earthquakes. A common and successful way is to dissipate excessive kinetic energy of structures via various damping devices, e.g. viscous fluid dampers, visco-elastic dampers [1], friction dampers [2], metallic yield dampers [3], buckling-restrained braces [4], magneto-rheological (MR) fluid dampers [5-6],and so on [7-9]. In most situations, the mechanical energy is converted to heat, and thus energy dissipation is often associated with undesirable self-heating, especially for viscous fluid dampers and MR dampers which are sensitive to temperature change [10-11].

Meanwhile, energy harvesting from ambient vibration sources for self-powered microsystems has emerged as a prominent research area [12-13]. A variety of mechanisms or materials have been explored, including electromagnetic induction [14], piezoelectricity [15], electrostatic generation [16], dielectric elastomers [17]. In particular, a great effort has been dedicated to the alternative power supply to wireless sensor networks [18-25]. For example, Torah et al. [22] developed a prototype of wireless sensor nodes powered by a micro-generator. Sozonov et al. [23] conducted field monitoring of a highway bridge using wireless sensors powered by an EM generator that harvests the energy induced by passing vehicles. In addition, Miller et al. [24] developed a solar energy harvesting system to power Imote2 wireless sensor networks, and validated its effectiveness on a cable-stayed bridge in South Korea.

Considering the emerging need of renewable energy at remote sites, the conventional 'energy dissipation' strategy may not be an optimal structural control strategy. So far, rare attention has been paid to energy harvesting dampers. In vehicle industry, some researchers developed regenerative vehicle suspension system using either electro-rheologic fluid dampers or electric actuators [26-30]. For example, Suda and Shiiba [27] proposed a hybrid suspension system with active control and energy generation functions. Based on that, Nakano et al. [30] developed a self-powered active control system. Additionally, vibration damping as a result of piezoelectric energy harvesting has been studied [31-32]. In the field of civil engineering, although a great amount of kinetic energy associated with the vibrations of civil structures provides potentially green energy to wireless electronic devices, relevant research works have been rarely reported in this regard.

Therefore, this paper presents a study of linear electromagnetic (EM) devices, termed linear EM dampers, which convert structural vibration energy into electricity efficiently. EM dampers can work in passive, semi-active or active modes [28, 33-40]. For example, Palomera-Arias [35-36] utilized an EM device as a passive damper, and studied the modeling of EM damping coefficient and the feasibility of using it for building vibration control. Cheng and Oh [39] proposed to use an EM damper for semi-active multi-mode vibration control of cantilever beams. Kim et al. [28] investigated active vibration control of vehicle suspension system using an EM damper. Zhang and Ou [40] performed theoretical and experimental study on the active vibration control of two-story shear building using an EM mass damper.

Provided that electricity energy is properly stored in energy storage elements (e.g. supercapacitors and rechargeable batteries), EM dampers can provide a green and regenerative power supply to portable and wireless devices at remote sites, and can serve as a superior

structural element with both vibration control and energy harvesting functions. Therefore, this paper aims to investigate the feasibility of using EM dampers for the both purposes simultaneously. The EM damper connected with four representative electric circuits has been theoretically and experimentally investigated, with a focus on several major characteristics, namely parasitic damping, EM damping, energy conversion efficiency and output power. The modeling of the EM damper's characteristics is first established based on the principles of structural dynamics and electromagnetics. Moreover, a series of dynamic tests of a small-scale prototype EM damper at different loading frequencies and amplitudes were performed to experimentally characterize the EM damper and to verify the proposed model. The comparison between the modeling and testing results demonstrates that the modeling technique can well predict the dynamic behavior of the EM damper and energy harvesting circuits. The experimental study is followed by a brief discussion of the feasibility of using EM dampers in civil infrastructures for both vibration damping and energy harvesting.

## 2. Modeling of EM Damper

### 2.1 Configuration of EM Damper

A passive linear EM damper is essentially a permanent magnet linear motor which is able to produce electrical power from motions. Figure 1-(a) shows a typical configuration of a linear moving-magnet DC motor [36]. It is composed of two major components – a permanent magnet and coils. According to Faraday's Law, when the permanent magnet and coils move relative to each other, an electromotive force (emf) is generated in the coils; according to Lorentz Law, the emf produces a current if the circuit is closed, and consequently an EM force is exerted on the moving magnet. The EM damping force is always against the relative movement and converts a portion of vibration energy into electricity instead of heat.

## 2.2 Power Flow

According to the energy balance equation, the input energy to a structure subjected to dynamic external excitations is always equal to the summation of the kinetic energy of structural mass, the elastic strain energy, the dissipative energy caused by structural inherent damping, and the dissipative energy caused by passive dampers if any [7]. The last part of energy would be absorbed by the EM dampers if the structure is equipped with an EM dampers-energy harvesting (EMDEH) system. On the other hand, this part of power becomes input power $P_{\text{in}}$ to the EMDEH system,

$$P_{\text{in}} = F \cdot \dot{x} \tag{1}$$

where $F$ and $\dot{x}$ are the instantaneous damper force and the velocity of the moving magnet respectively. The input power is dissipated by two different damping effects of the EM dampers—parasitic damping power $P_{\text{p}}$ and EM damping power $P_{\text{em}}$. Parasitic damping arises due to various mechanical power losses when the EM dampers are in motion. In general, parasitic damping is independent with the current in circuit, and can be evaluated in an open-circuit situation. The other part of the input power, $P_{\text{em}}$, is transferred to electrical energy in the circuit in Figure 1-(b). EM damping arises only when the circuit is closed and the current flows in the circuit. Only a portion of electric power, termed output power $P_{\text{out}}$, can be finally stored in energy storage elements or be utilized by end instruments. The other part will be dissipated by the copper loss of the coil, $P_{\text{coil}}$, and the power loss induced by the energy harvesting circuit, $P_{\text{loss}}$. Figure 2 shows the power flow in a vibrating structure with EMDEH system. The energy balance equation can be written as:

$$P_{\text{in}} = P_{\text{p}} + P_{\text{em}} = P_{\text{p}} + P_{\text{coil}} + P_{\text{gross}} = P_{\text{p}} + P_{\text{coil}} + P_{\text{loss}} + P_{\text{out}} \tag{2}$$

where $P_{gross}$ is the gross output power from the EM dampers. EM dampers are more attractive than conventional passive dampers in civil infrastructures in the sense that EM dampers not only provide energy dissipation mechanism to mitigate structural vibration, but also enable energy harvesting from structural vibration. In Equation (1), all the terms represent the instantaneous powers. When the EM damper is subjected to a harmonic oscillation with constant displacement amplitude as described by

$$x = d\sin(2\pi ft) \tag{3}$$

where $x$ is the displacement time history, $d$ is the displacement amplitude and $f$ is the oscillation frequency, it is common to evaluate the average power in one cycle

$$\overline{P}_{\text{in}} = \frac{1}{T}\int_0^T P_{\text{in}} \cdot dt\,, \quad \overline{P}_{\text{p}} = \frac{1}{T}\int_0^T P_{\text{p}} \cdot dt\,, \quad \overline{P}_{\text{em}} = \frac{1}{T}\int_0^T P_{\text{em}} \cdot dt\,, \quad \overline{P}_{\text{out}} = \frac{1}{T}\int_0^T P_{\text{out}} \cdot dt \tag{4}$$

## 2.3 Parasitic damping

As aforementioned, parasitic damping arises due to various mechanical losses, e.g. friction loss, windage loss, magnetic loss (also known as iron loss), etc., when the linear EM damper oscillates. Usually the magnitude of parasitic damping cannot be overlooked, compared with the EM damping. Although modeling each loss separately is possible, it is often impractical to directly apply such complex modeling in dynamic analyses of civil structures with EM dampers. According to the observations in the testing, the parasitic damping is modeled by a superposition of two components—viscous damping and coulomb damping—in this study. These two damping forms are widely considered in dynamic analyses of civil structures. The latter one is a typical rate-independent damping form used to account for the friction effect. Under a harmonic excitation, the average power of parasitic damping can be estimated by:

$$\overline{P}_{\text{p}} = 4k_1 fd + 2k_2\pi^2 f^2 d^2 \tag{5}$$

where $k_1$ represents the magnitude of the friction force, and $k_2$ is the viscous damping coefficient. Based on the average power of parasitic damping $\overline{P}_{\mathrm{p}}$, the equivalent viscous damping coefficient $C_{\mathrm{p}}$ for the parasitic damping can be evaluated according to the equal energy dissipation rule:

$$\overline{P}_{\mathrm{p}} = \frac{1}{T}\int_0^T C_{\mathrm{p}}\dot{x}^2 dt \tag{6}$$

From Equations (5) and (6), the equivalent viscous damping coefficient for parasitic damping reads

$$C_{\mathrm{p}} = \frac{2k_1}{\pi^2 fd} + k_2 \tag{7}$$

where $k_1$ and $k_2$ are the constants to be evaluated using $\overline{P}_{\mathrm{p}}$. The equivalent viscous damping coefficient $C_{\mathrm{p}}$ varies with the frequency and amplitude of the harmonic oscillation because of the consideration of coulomb damping.

### 2.4 EM Damping

Figure 1-(b) shows an equivalent circuit of the EM damper, where the AC source $U_0$ represents the open-circuit voltage which is generated when the permanent magnet moves relative to the coils, and $L$ and $R_{\mathrm{coil}}$ represent the inductance and resistance of the coils. As derived from Faraday's law of induction, the back emf $e$ is proportional to the velocity of moving part in the EM dampers but opposite in sign [30]. Then the open circuit voltage $U_0$ is given by

$$U_0 = -e = K_{\mathrm{e}}\dot{x} \tag{8}$$

where $K_{\mathrm{e}}$ is the back emf constant (V·s/m) dependent on the geometric and magnetic properties of the EM dampers. Once the circuit is closed, the emf (i.e. open-circuit voltage) would drive a current $I_1$ to flow in the circuit, and according to Kirchhoff Voltage Law (KVL), we have

$$U_0 = L\dot{I}_1 + R_{\mathrm{coil}}I_1 + U_1 \tag{9}$$

Considering the typically low vibration frequencies of civil structures (e.g. 0.1 – 10 Hz) and the relative small value of $L$ of the tested damper, the effect of the coil inductance is ignored in this study unless otherwise stated. According to Lorentz law, an EM damping force proportional to the current in the coil would be exerted on the part in motion:

$$F_{\text{em}} = K_{\text{f}} I_1 \tag{10}$$

where $I_1$ is the current in the coil as shown in Figure 1-(b), and the proportional coefficient $K_{\text{f}}$ is force constant of the damper (N/A), which is equal to $K_{\text{e}}$. Hence $K = K_{\text{f}} = K_{\text{e}}$ are also known as the motor constant of liner-motion EM devices. The instantaneous power of the EM damping can be expressed by

$$P_{\text{em}} = F_{\text{em}}\dot{x} = U_0 I_1 \tag{11}$$

Similar to Equation (6), when the EM damper is subjected to a harmonic displacement, the equivalent viscous damping coefficient for the EM damping can be evaluated by

$$\overline{P}_{\text{em}} = \frac{1}{T}\int_0^T P_{\text{em}} dt = \frac{1}{T}\int_0^T C_{\text{em}}\dot{x}^2 dt \tag{12}$$

The maximum current $I_{1,\text{max}}$, often achieved by shorting the circuit, would lead to the maximum EM damping coefficient $C_{\text{em,max}}$. The total damping coefficient of the EM damper $C$ is the superposition of the parasitic damping and the EM damping:

$$C = C_{\text{p}} + C_{\text{em}} \tag{13}$$

## 2.5 Energy Conversion Efficiency

In addition to the above-mentioned power of the parasitic damping and the EM damping, the other power terms in Equation (2) can be computed by

$$P_{\text{coil}} = I_1^2 R_{\text{coil}} \tag{14}$$

$$P_{\text{gross}} = P_{\text{out}} + P_{\text{loss}} = U_1 I_1 = \frac{U_1(U_0 - U_1)}{R_{\text{coil}}} \tag{15}$$

where $P_{\text{loss}}$ stands for any power loss involved in the rectifier or energy harvesting circuits. The maximum instantaneous gross output power $P_{\text{gross,max}}$ occurs when $\mathrm{d}P_{\text{gross}}/\mathrm{d}U_1 = 0$, i.e.

$$\text{when } U_1 = \frac{U_0}{2}, \quad P_{\text{gross,max}} = \frac{U_0^2}{4R_{\text{coil}}} \tag{16}$$

Considering the average output power $\overline{P}_{\text{out}}$ when subjected to a harmonic excitation, the energy conversion efficiency $\eta$ of the EMDEH system is defined as:

$$\eta = \frac{\overline{P}_{\text{out}}}{\overline{P}_{\text{in}}} = \eta_1 \cdot \eta_2 \cdot \eta_3 \tag{17}$$

where $\eta_1$, $\eta_2$ and $\eta_3$ are three energy conversion ratios:

$$\eta_1 = \frac{\overline{P}_{\text{em}}}{\overline{P}_{\text{in}}} = \frac{\overline{P}_{\text{em}}}{\overline{P}_{\text{p}} + \overline{P}_{\text{em}}} = \frac{C_{\text{em}}}{C_{\text{p}} + C_{\text{em}}} \tag{18}$$

$$\eta_2 = \frac{\overline{P}_{\text{gross}}}{\overline{P}_{\text{em}}} = \frac{\int_0^T U_1 I_1 dt}{\int_0^T U_0 I_1 dt} \approx 1 - \frac{\int_0^T I_1^2 R_{\text{coil}} dt}{\int_0^T U_0 I_1 dt} \tag{19}$$

$$\eta_3 = \frac{\overline{P}_{\text{out}}}{\overline{P}_{\text{gross}}} = \frac{\overline{P}_{\text{out}}}{\overline{P}_{\text{out}} + \overline{P}_{\text{loss}}} \tag{20}$$

A small parasitic damping or a high motor constant can maximize the ratio $\eta_1$; a small resistance of the coil can maximize the ration $\eta_2$, and a high-efficiency circuit design can maximize the ratio $\eta_3$. In order to enhance overall energy conversion efficiency, we have to minimize the total power loss in EMDEH system, $\overline{P}_{\text{p}} + \overline{P}_{\text{coil}} + \overline{P}_{\text{loss}}$. It is noteworthy that the maximum output power $\overline{P}_{\text{out,max}}$ does not occur simultaneously with the maximum EM damping $C_{\text{em,max}}$; and furthermore, $\overline{P}_{\text{out,max}}$ may not be corresponding to the maximum energy conversion efficiency $\eta_{\max}$ under a

harmonic displacement excitation (as defined in Equation (3)), because the input power to the EM damper $\overline{P}_{\text{in}}$ is not constant.

### 2.6 Case Study

Given that $U_0$ is known, the magnitudes of $I_1$ and $U_1$ in Figure 1-(b) and Equation (9) significantly depend on the characteristics of the external circuit outside the EM damper, which hereby affects the vibration damping and energy harvesting features of the EMDEH system. Four representative circuits shown in Figure 3 are considered in this subsection. The damping coefficient, the output power and the energy harvesting efficiency are discussed based on the current-voltage relationship. As aforementioned, the coil inductance $L$ is considered small and ignorable.

#### *Case 1: Open Circuit*

In case 1, the circuit is open and the EM damper is not connected to any external electric load. As a result, we have

$$I_1 = 0\,, \quad U_1 = U_0 \tag{21}$$

$$C_{\text{em}} = 0\,, \quad C = C_{\text{p}}\,, \quad P_{\text{in}} = P_{\text{p}} \tag{22}$$

Therefore, the parasitic damping and the open-circuit voltage could be studied in this case through the cyclic behavior of the EM damper.

#### *Case 2: Circuit with Constant Resistor*

In case 2, the external electric load is a resistor of a constant resistance $R_{\text{load}}$. The Equation (9) can be rewritten as

$$I_1 = \frac{U_0}{R_{\text{coil}} + R_{\text{load}}} \tag{23}$$

From Equations (8) and (10), we have

$$F_{\text{em}} = \frac{K^2}{R_{\text{coil}} + R_{\text{load}}} \dot{x} \tag{24}$$

$$C_{\text{em}} = \frac{K^2}{R_{\text{coil}} + R_{\text{load}}} \tag{25}$$

Equation (25) is reported by [41] as well. As shown by Equation (24), the EM damping force is proportional to the velocity, and thus the EM damping can be viewed as linearly viscous damping when the EM damper is connected to a resistor alone. Moreover, the EM damping coefficient can be easily changed by adjusting the external resistance $R_{\text{load}}$. Obviously, the maximum EM damping can be achieved in the situation of a short circuit, i.e.

$$C_{\text{em,max}} = K^2 / R_{\text{coil}} \quad \text{when } R_{\text{load}} = 0 \tag{26}$$

The average parasitic damping power in one cycle is given by Equation (5). On the other hand, based on Equation (12), the average EM damping power in one cycle can be rewritten as

$$\overline{P}_{\text{em}} = \frac{2\pi^2 f^2 d^2 K^2}{R_{coil} + R_{load}} = \frac{U_m^2}{2(R_{coil} + R_{load})} \tag{27}$$

where $U_m = 2\pi f d K$ is the peak open-circuit voltage under a harmonic displacement excitation. The average input power to the EMDEH system can be evaluated by Equations (2), (5) and (27). If we consider that the power consumption by $R_{\text{load}}$ is the output power, no power loss arises in the external circuit, i.e. $\eta_3 = 1$. The instantaneous output power is

$$P_{\text{out}} = U_1 I_1 = \frac{K^2 R_{\text{load}}}{(R_{\text{coil}} + R_{\text{load}})^2} \dot{x}^2 \tag{28}$$

The maximum output power is as follows

$$P_{\text{out,max}} = \frac{K^2}{4R_{\text{coil}}} \dot{x}^2 \quad \text{when } R_{\text{coil}} = R_{\text{load}} \text{ and } U_1 = U_0 / 2 \tag{29}$$

Consistent with the observation by [36, 42], the maximum output power occurs at impedance matching (i.e. $R_{\text{coil}} = R_{\text{load}}$ ). This is consistent with the observation by. When the EM damper is subjected to a harmonic oscillation, the average output power could be computed from Equations (3), (4), (28) and (29):

$$\overline{P}_{\text{out}} = \frac{2\pi^2 f^2 d^2 K^2 R_{\text{load}}}{(R_{\text{coil}} + R_{\text{load}})^2} = \frac{U_m^2 R_{\text{load}}}{2(R_{\text{coil}} + R_{\text{load}})^2} \tag{30}$$

$$\overline{P}_{\text{out,max}} = \frac{\pi^2 f^2 d^2 K^2}{2R_{\text{coil}}} = \frac{U_m^2}{8R_{\text{coil}}} \tag{31}$$

From Equation (19), the energy conversion ratio $\eta_2$ is

$$\eta_2 = \frac{U_1}{U_0} = \frac{R_{\text{load}}}{R_{\text{coil}} + R_{\text{load}}} \tag{32}$$

When the coil resistance is much less than the external resistance, i.e. $R_{\text{coil}} << R_{\text{load}}$ , the $\eta_2$ approaches the upper limit $\eta_2 \approx 1$ . Nevertheless, the maximum output power $P_{\text{out,max}}$ corresponds to $\eta_2 = 0.5$. The overall energy conversion efficiency is

$$\eta = \eta_1 \cdot \eta_2 \cdot \eta_3 = \frac{C_{\text{em}}}{C_{\text{p}} + C_{\text{em}}} \cdot \frac{R_{\text{load}}}{R_{\text{coil}} + R_{\text{load}}} = \frac{K^2 \alpha}{C_{\text{p}} R_{\text{coil}} (1+\alpha)^2 + K^2 (1+\alpha)} \tag{33}$$

where $\alpha = R_{\text{load}} / R_{\text{coil}}$. The optimal energy conversion efficiency occurs when $\mathrm{d}\eta / \mathrm{d}\alpha = 0$, i.e.

$$\text{when } \alpha_{\text{opt}} = \sqrt{1 + \frac{K^2}{C_{\text{p}} R_{\text{coil}}}} \Rightarrow \eta_{\max} \tag{34}$$

Equation (7) implies that the parasitic damping coefficient $C_{\text{p}}$ is dependent on the vibration frequency and amplitude, if the coulomb damping is considered. Therefore, the optimal value $\alpha_{\text{opt}}$ also depends on the frequency, amplitude and the values of $k_1$ and $k_2$:

when $k_1 \to \infty$ or $f \to 0$ or $d \to 0$

$$C_{\mathrm{p}} = \infty, \qquad \alpha_{\mathrm{opt}} = 1, \qquad \eta_{\max} = 0$$

$$\text{when } k_1 \to 0 \text{ or } f \to \infty \text{ or } d \to \infty \tag{35}$$

$$C_{\mathrm{p}} = k_2, \qquad \alpha_{\mathrm{opt}} = \sqrt{1 + K^2 / k_2 R_{\mathrm{coil}}} > 1$$

$$\eta_{\max} = \frac{K^2 \alpha_{\mathrm{opt}}}{k_2 R_{\mathrm{coil}} (1 + \alpha_{\mathrm{opt}})^2 + K^2 (1 + \alpha_{\mathrm{opt}})}$$

In general, the optimal value $\alpha_{\mathrm{opt}}$ is greater than 1 and the maximum energy conversion efficiency $\eta_{\max}$ increases with the frequency and amplitude of the displacement oscillation. Figure 4 illustrates an example of the variations of $\overline{P}_{in}$, $\overline{P}_{em}$, $\overline{P}_{out}$, $\eta_1$, $\eta_2$ and $\eta$ with the parameter $\alpha$ in case 1. The corresponding parameters in this example are consistent with those used in the next section ($K$=7.474 V·s/m, $R_{\mathrm{coil}}$=4Ω, $f$=6Hz, $d$=11mm). It can be seen that the energy conversion ratios $\eta_1$ monotonically decreases with the parameter $\alpha$, while $\eta_2$ monotonically increases. The overall energy conversion efficiency $\eta$ has a maximum value when $\alpha$=1.99, according to Equation (34). On the other hand, the optimal output power $\overline{P}_{out,\max}$ occurs when $\alpha$=1, as implied by Equation (29). Apparently, the optimal output power does not occur simultaneously with the maximum energy conversion efficiency, because $\eta$ is defined as the ratio of $\overline{P}_{out} / \overline{P}_{in}$ and the input power $\overline{P}_{in}$ does not keep constant with the varying parameter $\alpha$. Figure 5 shows the variation of peak damper force and optimal output power (corresponding to $\alpha$=1) with the increase of excitation frequency. As predicted by Equations (24), (29) and (31), the peak damper force is proportional to the frequency, while the optimal output power is proportional to the square of the frequency.

### *Case 3: Circuit with Rectifier and Supercapacitor*

In case 3, the EM damper is equipped with a simple energy harvesting circuit, comprising a full-wave rectifier, a supercapacitor and a resistor. In this circuit the electricity produced by the EM damper can be stored in the supercapacitor and be further utilized to power some electric devices. The full-wave rectifier composed of four diodes is used to convert AC power produced by the EM damper to DC power. The resistor shown in Figure 3-(c) stands for the power consumption of any electric devices. Supercapacitors, like rechargeable batteries, are common energy storage elements. Supercapacitors refer to a special type of capacitors with a very high capacitance (1-100F) and a very low withstandable voltage [21]. The stored electric energy in a supercapacitor is [42]

$$E_{\mathrm{C}} = \frac{1}{2} C U_C^2 \tag{36}$$

where $C$ is the capacitance; $U_{\mathrm{C}}$ is the voltage of the supercapacitor. Figure 6-(a) shows that the voltage $U_{\mathrm{C}}$ rises with the increase of the stored energy.

The use of a diode is always associated with a constant conduction voltage $\mathrm{V_F}$ (0.2- 0.7 V) which leads to the power loss in the EMDEH system. This voltage drop should not be neglected unless the emf is considerably greater than $\mathrm{V_F}$. Owing to the full-wave rectifier, the current in Figure 3-(c) is converted to DC. Assume the instantaneous voltage of the supercapacitor is $U_{\mathrm{C}}$, then the current $I_1$ is non-zero only when $|U_0|$ produced by the EM damper is greater than the cut-in voltage $2V_{\mathrm{F}} + U_{\mathrm{C}}$:

$$I_1 = \begin{cases} 0 & \text{when } \left|U_0\right| \le 2V_F + U_c \\ (U_0 - 2V_F - U_c)/R_{\mathrm{coil}} & \text{when } U_0 > 2V_F + U_c \\ (U_0 + 2V_F + U_c)/R_{\mathrm{coil}} & \text{when } U_0 < -(2V_F + U_c) \end{cases} \tag{37}$$

where the equivalent series resistance of the supercapacitor is considered to be small and negligible. From Equations (8), (10) and (37), the EM damping force $F_{\text{em}}$ is given by

$$F_{\text{em}} = \begin{cases} 0 & \text{when } |\dot{x}| \le \dot{x}_{\text{cut-in}} \\ K^2/R_{\text{coil}}\,(|\dot{x}| - \dot{x}_{\text{cut-in}}) & \text{when } \dot{x} > \dot{x}_{\text{cut-in}} \\ -K^2/R_{\text{coil}}\,(|\dot{x}| - \dot{x}_{\text{cut-in}}) & \text{when } \dot{x} < -\dot{x}_{\text{cut-in}} \end{cases} \tag{38}$$

where $\dot{x}_{\text{cut-in}}$ is the cut-in velocity defined by $\dot{x}_{\text{cut-in}} = (2V_{\text{F}} + U_{\text{C}})/K$. Equation (38) implies that the EM damping force vs. velocity relationship becomes nonlinear, and thus the EM damping is no longer linear viscous damping in case 3. Then the total damper force of the EM damper can be approximately estimated by

$$F = \begin{cases} C_{\text{p}}\dot{x} & \text{when } |\dot{x}| \le \dot{x}_{\text{cut-in}} \\ K^2/R_{\text{coil}}\,(|\dot{x}| - \dot{x}_{\text{cut-in}}) + C_{\text{p}}\dot{x} & \text{when } \dot{x} > \dot{x}_{\text{cut-in}} \\ -K^2/R_{\text{coil}}\,(|\dot{x}| - \dot{x}_{\text{cut-in}}) + C_{\text{p}}\dot{x} & \text{when } \dot{x} < -\dot{x}_{\text{cut-in}} \end{cases} \tag{39}$$

If the damper is subjected to the harmonic displacement in Equation (3), the EM damping power and the equivalent EM damping coefficient $C_{\text{em}}$ can be evaluated from Equation (12):

$$\overline{P}_{em} = \frac{1}{T}\int_0^T C_{\text{em}}\dot{x}^2 dt = \frac{U_m^2}{\pi R_{\text{coil}}}(\cos^{-1}\Gamma - \Gamma\sqrt{1-\Gamma^2}) \tag{40}$$

$$C_{\text{em}} = \frac{\overline{P}_{\text{em}}}{\int_0^T \dot{x}^2 dt / T} = \frac{2K^2}{\pi R_{\text{coil}}}(\cos^{-1}\Gamma - \Gamma\sqrt{1-\Gamma^2}) \tag{41}$$

where $\Gamma = (2V_{\text{F}} + U_{\text{C}})/2\pi fdK$ $(0 \le \Gamma \le 1)$, and $U_{\text{m}}$ is the maximum open-circuit voltage during the harmonic oscillation, $U_{\text{m}} = 2\pi fd \cdot K$. With a given harmonic excitation, the EM damping coefficient is a function of $U_{\text{C}}$. It should be pointed out that the voltage of the supercapacitor $U_{\text{C}}$ varies over time. Since the supercapacitor has a large capacitance C, the voltage fluctuation in one cycle is usually minimal and can be ignored. However, $U_{\text{C}}$ rises during the charge process

from 0V to $U_m - 2V_F$ if the switch in Figure 3-(c) is open. The increase of $U_C$ will lead to the monotonic reduction of the EM damping. For example, when the supercapacitor is uncharged ($U_C$ = 0), the current $I_1$, the EM damping force $F_{em}$ and the EM damping coefficient $C_{em}$ are maximum. However, $C_{em,max}$ is less than the counterpart in case 2 (see Equation (26)), because of the voltage drop induced by the rectifier circuit. On the other hand, $I_1$, $F_{em}$ and $C_{em}$ are all equal to zero when the supercapacitor reaches the highest voltage $U_m - 2V_F$ (corresponding to $\Gamma = 1$).

In this case, the power stored in the supercapacitor and consumed by the load is considered as the output power. The full-wave rectifier converts the AC to the DC, i.e. $I_2 = |I_1|$. Meanwhile, the voltage drop of the diodes is associated with the power loss. The instantaneous power loss and output power are

$$P_{loss} = 2V_F \cdot |I_1| \tag{42}$$

$$P_{out} = U_C \cdot |I_1| \tag{43}$$

Under the harmonic displacement history specified in Equation (3), the average output power in one cycle can be evaluated by integration

$$\overline{P}_{loss} = \frac{1}{T}\int_0^T 2V_F \cdot |I_1| dt = \frac{4V_F U_m}{\pi R_{coil}}(\sqrt{1-\Gamma^2} - \Gamma\cos^{-1}\Gamma) \tag{44}$$

$$\overline{P}_{out} = \frac{1}{T}\int_0^T U_C |I_1| dt = \frac{2(\Gamma U_m - 2V_F)U_m}{\pi R_{coil}}(\sqrt{1-\Gamma^2} - \Gamma\cos^{-1}\Gamma) \tag{45}$$

where $U_m$ and $\Gamma$ are defined before. The maximum average output power in one cycle occurs when $d\bar{P}_{out}/d\Gamma = 0$, i.e.

$$\text{when } (\Gamma U_m - 2V_F)\cos^{-1}\Gamma = U_m(\sqrt{1-\Gamma^2} - \Gamma\cos^{-1}\Gamma) \quad \Rightarrow \quad \Gamma_{opt} = 0.4 + 1.2V_F/U_m \tag{46}$$

where the latter one is an approximately numerical solution to the transcendental equation. The corresponding optimal average output power is

$$\overline{P}_{\text{out,max}} = \frac{0.255(U_m - 2V_F)U_m}{R_{coil}}(\sqrt{1-\Gamma_{opt}^2} - \Gamma_{opt}\cos^{-1}\Gamma_{opt}) \tag{47}$$

It is not surprising that the voltage drop of the diodes influences the effective output power, and hence a smaller $V_F$ is always desirable. If $V_F \ll U_m$, the voltage drop and the associated power loss can be ignored then we have

$$\text{If } V_F \ll U_m,\ \overline{P}_{out,\max} \approx 0.115\frac{U_m^2}{R_{coil}} \tag{48}$$

Compared with Equation (31) in case 1, the maximum output power is smaller even if the power loss of the diodes is neglected, because the non-zero cut-in voltage makes the duty cycle less than 1. The input power to the EMDEH system is $\overline{P}_{\text{in}} = \overline{P}_{\text{p}} + \overline{P}_{\text{em}}$. With $\eta_1$ given by Equation (18), the other intermediate energy conversion ratios and the overall energy conversion efficiency can be calculated from Equations (17), (19) and (20)

$$\eta_2 = \frac{2\Gamma\sqrt{1-\Gamma^2} - 2\Gamma^2\cos^{-1}\Gamma}{\cos^{-1}\Gamma - \Gamma\sqrt{1-\Gamma^2}} \tag{49}$$

$$\eta_3 = 1 - \frac{2V_F}{\Gamma U_m} \tag{50}$$

$$\eta = \eta_1 \cdot \eta_2 \cdot \eta_3 = \frac{4K^2(\Gamma U_{\text{m}} - 2V_F)\cdot(\sqrt{1-\Gamma^2} - \Gamma\cos^{-1}\Gamma)}{C_{\text{p}}R_{\text{coil}}\pi U_{\text{m}} + 2K^2U_{\text{m}}(\cos^{-1}\Gamma - \Gamma\sqrt{1-\Gamma^2})} \tag{51}$$

The maximal energy conversion efficiency is achieved when $d\eta/d\Gamma = 0$. Figure 7 illustrates the theoretical variation of $\overline{P}_{in}$, $\overline{P}_{em}$, $\overline{P}_{loss}$, $\overline{P}_{out}$, $\eta_1$, $\eta_2$, $\eta_3$ and $\eta$ with the parameter $U_C$ or $\Gamma$ in case 3. The corresponding parameters are consistent with those of the small-scale EM damper described and tested in the next section ($K$=7.474 V.s/m, $R_{\text{coil}}$=4Ω, $f$=6Hz, $d$=11mm, $V_F$=0.22V). It can be

seen that the overall energy conversion efficiency $\eta$ has a maximum value when Γ=0.602 ($U_C$ = 1.43V) as shown in Figure 7-(b), while the optimal output power $\overline{P}_{out,max}$ occurs when Γ=0.485 ($U_C$ = 1.06V) as predicted by Equation (46). Similar to case 2, the optimal output power does not correspond to the maximum energy conversion efficiency because the input power $\overline{P}_{in}$ is not constant with the varying parameter Γ. Moreover, Figure 8 shows the variation of the maximal output power, and its corresponding parameters $\Gamma_{opt}$, $\eta$ and $C_{em}$ with the increasing $U_m$. As implied by Equation (46), the effect of conduction voltage of diodes $V_F$ becomes smaller and $\Gamma_{opt}$ approaches 0.4 with the increase of $U_m$. Figure 9 shows the variation of peak damper force and optimal output power (when $\Gamma = \Gamma_{opt}$) with the excitation frequency. In general, the peak damper force and the optimal output power show the linear and quadratic growth trends respectively with the increase of frequency, except the part corresponding to a relatively low frequency. At a low frequency, the peak velocity is low and the open circuit voltage is less than the cut-in voltage. As a result, the EM damping and the output power is equal to zero. It needs to be noted that in real applications, the motor constant and open circuit voltage of EM dampers are much greater than the values of the small-scaled dampers in this paper. If $V_F << U_m$, the voltage drop of diodes will have minimal effect on the output power.

The above discussion indicates that $C_{em}$, $\overline{P}_{out}$ and $\eta$ are all dependent on the supercapacitor voltage $U_C$ (or the parameter Γ). $C_{em,max}$ occurs when $U_C$=0, while $\overline{P}_{out,max}$ and $\eta_{max}$ correspond to some specific values of $U_C$. The supercapacitor voltage $U_C$ rises during the charge process from 0V to a steady value $U_{C,max}$. It is noteworthy that the steady value that can be achieved is determined by the load resistance. If the switch is open, the maximum voltage of the supercapacitor is equal to $U_m - 2V_F$. If $R_{load}$ is very small, it is possible that $U_{C,max}$ is less than

$\Gamma_{opt}$ in Equation (46) and the optimal output power cannot be achieved. In this situation, the maximum average output power corresponds to $U_{C,max}$ during the charge process.

### *Case 4: Circuit with Rectifier and Rechargeable Battery*

In case 4, the energy storage utilizes a rechargeable battery instead of a supercapacitor. All the other conditions are the same as case 3. Examples of rechargeable batteries include Li-ions, NiMH, NiCd, SLA, Li Polymer, etc [21]. Figure 6-(b) shows a typical charge curve for NiMH battery, in which $U_n$ stands for the nominal voltage of the NiMH battery. If an empty battery is charged, the voltage rises quickly to $U_n$. The maximum voltage of the NiMH battery, if fully charged, is about 15~20% higher than its nominal voltage. Compared with a supercapacitor, the voltage of a rechargeable battery is more stable during the charge process. As mentioned above, the variation of the voltage of energy storage elements results in the change in the EM damping and the energy harvesting efficiency. Therefore, the relative stable voltage is desirable in consideration of controlling the damping property of the EM damper. In addition, rechargeable batteries have lower self-discharge rate and higher energy density than supercapacitors [43]. However, it should be pointed out as well that rechargeable batteries usually have stringent charge requirements in order to avoid potential overcharge that may damage the batteries; while supercapacitors are able to withstand very high charge and discharge rate, and require relatively simple charge methods. Besides, supercapacitors do not suffer from memory effects like some batteries, and virtually they have very long life. In addition to the above-mentioned factors, the discussions of the EM damping and energy harvesting are similar to case 3. Equations (37)~(51) are applicable in case 4 as well.

## 3. Experimental Study

A non-commutated DC linear servo motor was cyclically tested as a small-scale EM damper on a MTS universal testing machine. Figure 1-(a) shows the configuration of the EM damper purchased from Baldor Motion Products. The damper has a diameter of 38.1 mm and a total length of 108.1 mm. The number of turns per coil and the wire diameter were estimated to be 270 and 24AWG, respectively, and the length of each coil and the magnet is 38 mm and 25 mm, respectively [36]. The measured coil resistance is 4.0Ω. During the testing, the four circuits described in the last section were connected to the EM damper individually. A series of sinusoidal displacements were applied at different frequencies (0.1 - 8 Hz) and different amplitudes (3, 6 and 11 mm). The responses of interest were measured by KYOWA EDX-100A data acquisition system with a sampling frequency of 500Hz, including the force, displacement, voltages and currents. Figure 10 shows the EM damper under test and the circuit on a breadboard corresponding to case 3. A full-wave rectifier comprising four Schottky diodes is used, as Schottky diodes are associated with much smaller forward voltage drop [21]. The measured $V_F$ of the Schottky diodes is equal to 0.22V in this experiment. The testing is intended to provide the validation of the afore-described modeling. The damping and energy harvesting behaviors were examined in each case.

### *Case 1: Open Circuit*

No current flows in an open circuit, associated with zero EM damping. Therefore, the parasitic damping and the open-circuit voltage can be studied. The voltage across two terminals was measured in this Case. Figure 11, containing the test data at different frequencies and amplitudes, illustrates the relationship between the open-circuit voltage (i.e. emf) and the oscillation velocity.

The nearly linear relation shown above is consistent with the prediction by Equation (8). The motor constant $K$ was identified as 7.474 V·s/m (or N/A) via a linear regression analysis.

Figure 12 shows the experimental relationship of the damper force and velocity at the frequency of 2 Hz and the displacement amplitude of 11 mm. As mentioned in section 2.3, the parasitic damping is modeled by a superposition of two components–viscous damping and coulomb damping. The latter is evidenced by the non-zero damper force at zero velocity in Figure 12. Figure 13 shows the testing results of the average power of parasitic damping in one cycle, $\overline{P}_{\mathrm{p}}$, for different frequencies and amplitudes. Subsequently, the two constants in Equation (5) are evaluated ($k_1$=0.4994 N, $k_2$=3.126 N·s/m) by a regression analysis using the testing data shown in Figure 13. The prediction by the simplified modeling presented in section 2.3 can match the experimental results very well.

### *Case 2: Circuit with Constant Resistor*

In Case 2, the EM damper under test was connected to a resistor which represents a general electric load. The measured coil resistance $R_{coil}$ is equal to 4.0Ω. Nine different resistors, namely 0Ω, 1.0Ω, 2.0Ω, 3.0Ω, 3.75Ω, 5.0Ω, 7.5Ω, 15.0Ω and 45.0Ω, were tested at different frequencies and amplitudes. In fact, Case 1 can be viewed as a special case of Case 2 with $R_{load}=\infty$. The current flowing in the circuit produces the EM damping force applied on the damper. Therefore, the damper force should be a result of the parasitic damping force plus the EM damping force. Figure 14 shows the experimental results of the damper's force-displacement relationship at the frequency of 6 Hz and the amplitude of 6 mm. As the parasitic damping is independent with the current in the circuit, Figure 14 implies that the EM damping is governed by the varying load

resistance in this case. Figure 15 illustrates the variation of the EM damping coefficient $C_{em}$ with the increase of $R_{load}$ for both the testing and modeling results. The testing data were computed by subtracting the parasitic damping coefficients $C_p$ from the total damping coefficients $C$, both obtained from regression analyses of the experimental force-velocity relation. A good match is noted between the experiment results and the theoretical prediction by Equation (25). Both the testing and modelling results demonstrate that the EM damping coefficient $C_{em}$ decreases monotonically with the increase of load resistance $R_{load}$, and the maximum value corresponds to a short circuit ($R_{load}$=0Ω). Moreover, Figures 14 and 15 imply that the damping feature of the EM damper can be conveniently controlled by tuning the value of $R_{load}$.

Based on Equation (4), the average output power, i.e. the power consumption of $R_{load}$, is calculated by the measured current and voltage on the electric load, and the average input power is calculated from the measured force and displacement. Subsequently, the energy conversion efficiency η can be calculated according to Equation (17). Figure 16 shows the variation of the average output power $\overline{P}_{out}$ with the parameter $\alpha = R_{load}/R_{coil}$ for two frequencies and three amplitudes, and Figure 17 shows the overall energy conversion efficiency η. The theoretical predictions by Equations (30) and (33) can match the experimental results fairly well in the two Figures. The testing results clearly indicate that the maximum output power occurs when $\alpha = 1$ ($R_{load}= R_{coil}$=4Ω), consistent with the prediction by Equation (29). The maximum average output power corresponding to $f$ = 6Hz and $d$ = 11 mm is around 274.3 mW. Meanwhile, the optimal energy conversion ratio ranges from 14.4% to 33.1%, depending on the frequency and amplitude. Table 1 presents the detailed comparison of the testing and modeling results regarding the optimal output power and the optimal energy conversion efficiency. It is noted in Figures 16 and

17 that the optimal value of α for the energy conversion efficiency (α>1) does not correspond to that for the output power (α=1).

### *Case 3: Energy Harvesting using Supercapacitor*

In case 3, a simple energy harvesting circuit consisting of a Schottky rectifier and a supercapacitor was tested. The supercapacitor (manufacturer: Nichicon, model number: JUC0E475MHD) has a capacitance value of 4.7F and an equivalent series resistance of 0.5 Ω. Five different resistors, $R_{load}$=1Ω, 2Ω, 4Ω, 15Ω, 30Ω, were used to simulate the power consumption of electric devices. The output power is defined as the power stored in the supercapacitor plus the power consumption of the resistor. Figure 18 shows the experimental time histories of the supercapacitor voltage $U_C$, the EM damping $C_{em}$, the output power $\overline{P}_{out}$ and the energy conversion efficiency η corresponding to $f$=6Hz and $d$=11mm. In Figure 18, Curve I shows the testing results with open switch (no electric load), and Curve II is for $R_{load}$=15Ω. In general, the voltage of the supercapacitor rises within the charging process until it reaches a steady value. However, the final steady voltage not only depends on the peak emf $U_m$, but also on the load resistance $R_{load}$, as observed in Figure 18. A smaller resistance stands for larger power consumption in the test; as such it corresponds to a slower charge process and a smaller steady voltage. The increase of the supercapacitor voltage $U_C$ leads to the variations of the three parameters—$C_{em}$, $\bar{P}_{out}$ and η—during the charge process. If the switch is open, the current passing the supercapacitor becomes minimal when $U_C$ reaches the final steady value. Accordingly, the EM damping coefficient, output power and energy conversion ratio are nearly zero in the steady state; if $R_{load}$=15Ω, the current passes the resistor even in the steady state, and consequently the corresponding EM damping coefficient, output power and energy conversion ratio are not equal to zero.

As shown in Figures 18-(d), 19 and 20, the EM damping keeps decreasing during the charge process even though $R_{load}$ is constant; the maximum damping coefficient $C_{em,max}$ occurs at $U_C$=0Ω, where $C_{em}$ is calculated by Equation (41). Figure 19 illustrates the experimental relationships of the damper force vs. the oscillation velocity, and the testing results are consistent with the prediction by Equation (39). The force-velocity relation is nonlinear due to the cut-in velocity/voltage, and is time-variant due to the change of $U_C$. On the other hand, the variation of the average output power $\overline{P}_{out}$ and the energy conversion efficiency η with the supercapacitor voltage $U_C$ is not monotonic. Figure 21 shows the experimental and theoretical relationships of the output power $\overline{P}_{out}$ vs. the supercapacitor voltage $U_C$ (or the parameter Γ), and Figure 22 shows the energy conversion efficiency η. It is seen that the theoretical curves in both Figures are independent with the load resistance $R_{load}$. However, $R_{load}$ affects the final peak $U_C$ that is achievable. The optimal output power $\overline{P}_{out,max} = 184\,\text{mW}$ occurs when $U_C$=1.06V (Γ=0.49) according to Equations (46) and (47); while the optimal energy conversion efficiency $\eta_{max} = 23\%$ corresponds to $U_C$=1.45V (Γ=0.61) according to Equation (51). Both the optimal power and energy efficiency are smaller than the counterparts in Case 2, because of the power loss on the diodes and the duty cycle less than 1. Figures 20-22 also demonstrate that the final steady voltage of the supercapacitor for $R_{load}$=15Ω is smaller than that for open switch. Again, the theoretical modeling closely matches the experimental results in Figures 20-22.

### *Case 4: Energy Harvesting using Rechargeable Battery*

In Case 4, a 1.2V NiMH battery (manufacturer: Varta, model number: 55625) with a capacity of 250 mAh is used as the energy storage element. Figure 23 shows some experimental results in

Case 4. Similar observations to Case 3 can be made to both experimental and theoretical results. However, the voltage of the rechargeable battery rises to 1.4 V quickly and stays almost unchanged afterwards. This leads to the much more stable EM damping $C_{em}$, output power $\overline{P}_{out}$ and energy conversion efficiency η during the charge process than Case 3 with the supercapacitor. It is noted that too small load resistance would cap the maximum voltage $U_{C,max}$, and thus the battery cannot be properly charged if $U_{C,max}$ is less than the nominal voltage of the battery.

## 4. Discussion

(a) As pointed out by [35], a part of energy dissipation occurs outside the EM damper, which may reduce the problems normally associated with the self-heating of viscous and friction dampers.

(b) Provided that the EM damper is connected to a variable resistor, the EM damping coefficient can be controlled by adjusting the resistance in the circuit. Therefore, the EM damper can function as a semi-active damper with variable damping property in structural control applications. Compared with variable-orifice viscous dampers, adjusting resistance can be more conveniently realized by a control circuit.

(c) The EM damper provides both vibration control and energy harvesting functions. The maximum output power of the tested small-scale EM damper ranges from several mW to 274mW. Considering the real scale of civil structures, the power that can be harvested from energy dissipation devices would be considerably larger. The typical power consumption of commercially available wireless sensors is 24 to 570 mW [24]. Therefore, the EM dampers have a potential to power a number of wireless sensors in real structures.

(d) As indicated in this study, the maximum damping coefficient of the EM damper does not correspond to the maximum output power. If the EM damper is intended for both vibration damping and energy harvesting, a trade-off strategy or an adaptive strategy should be taken in the future design of EMDEH system.

(e) The damping property of the EM damper may be subjected to noticeable variation during the charge process. This fact may complicate the solution of optimal damping, and thus should be paid enough attention in the design procedure.

(f) In addition to the energy harvesting capability, there exist simple relationships between the emf and the velocity, and between the current and the EM damping force. Both the voltage and current are signals easily to be measured. It is promising to build a self-sensing self-powered semi-active vibration control system using the EM damper.

## 5. Conclusions

To examine the feasibility of using EM dampers in civil infrastructures for both vibration damping and energy harvesting, this paper presents the modeling and testing of the EMDEH system. The theoretical model is built based on the fundamentals of structural dynamics and electromagnetics. In particular, four representative electric circuits are considered in this study, namely an open circuit, a circuit with a constant resistor, a circuit with a full-wave rectifier and a supercapacitor, and a circuit with a full-wave rectifier and a rechargeable battery. Some main dynamic characteristics and their optimal values are discussed in details in this procedure, including the parasitic damping, the EM damping, the energy harvesting efficiency and the effective output power. The effectiveness of the proposed modeling is validated by a series of dynamic tests of a small-scale EM damper performed at different frequencies and amplitudes. A

good match clearly demonstrates that the modeling can predict the mechanical and electrical behavior of the EMDEH system very well.

Both the theoretical and experimental results indicate that the EM damping and energy harvesting features are considerably influenced by the external circuit connected to the damper. The EM damping is similar to viscous fluid damping when the damper is connected to a constant resistor; while the relationship of the EM damping force vs. velocity becomes nonlinear when the damper is connected to a rectifier and an energy storage element such as a supercapacitor or a rechargeable battery. In the latter case, both the damping coefficient and the energy conversion efficiency vary to some extent with the voltage increase during the charge process. Furthermore, the maximum damping and the maximum output power cannot be achieved simultaneously, and thus a trade-off strategy needs to be made in the design if the EM dampers are intended for both vibration damping and energy harvesting functions.

Considering the real scale of civil infrastructures, it is promising to use EM dampers to mitigate structural vibration and power some potable and wireless electric devices simultaneously. As the mechanical behavior of EM dampers is similar to that of viscous fluid dampers, EM dampers could replace traditional viscous fluid dampers in vibration mitigation of lightly damped and flexible structures, such as high-rise buildings and stay cables. It should be pointed out that the relatively simple energy harvesting circuits are considered in this study. In practice, the energy harvesting architecture may include more complex components, e.g. power conditioning and monitoring. The addition of these components may affect both damping and energy conversion. All of these need to be investigated in future study.

## Acknowledgement

The authors are grateful for the financial support from the Research Grants Council of Hong Kong through a GRF grant (Project No. 533011). Findings and opinions expressed here, however, are those of the authors alone, not necessarily the views of the sponsor.

## References:

[1] Shen KL, Soong TT, Chang KC, Lai ML. Seismic behavior of reinforced concrete frame with added viscoelastic dampers. Eng Struct 1995;17(5):372–80.

[2] Xu YL, Chen B. Integrated vibration control and health monitoring of building structures using semi-active friction dampers: Part I—methodology. Eng Struct 2008; 30(7): 1789-1801.

[3] Ghabraie K, Chan R, Huang XD, Xie YM. Shape optimization of metallic yielding devices for passive mitigation of seismic energy. Eng Struct 2010; 32(8):2258-2267.

[4] Sabelli R, Mahin S, Chang C. Seismic demands on steel braced frame buildings with buckling-restrained braces. Eng Struct 2003; 25(5):655-666.

[5] Yang G, Spencer BF, Carlson JD, Sain MK. Large-scale MR fluid dampers: modeling and dynamic performance considerations. Eng Struct 2002; 24(3):309-323.

[6] Ni YQ, Chen Y, Ko JM, Cao DQ. Neuro-control of cable vibration using semi-active magneto-rheological dampers. Eng Struct 2002; 24(3):295-307.

[7] Soong TT, Dargush GF. Passive energy dissipation system in structural engineering. John Wiley & Sons Ltd. Chichester, England;1997.

[8] Housner GW, Bergman LA, Caughey TK, Chassiakos AG, Claus RO, Masri SF, Skelton RE, Soong TT, Spencer BF, Yao JTP. Structural control: past, present, and future. J Engng Mech 1997; 123(9): 897-971.

[9] Soong TT, Spencer BF. Supplemental energy dissipation: state-of-the-art and state-of-the-practice. Engng Struct 2002;24: 243-259.

[10] Makris N, Roussos Y, Whittaker AS, Kelly JM. Viscous heating of fluid dampers. II: large-amplitude motions. J Engng Mech, ASCE 1998;124(11): 1217-1223.

[11] Gordaninejad F, Breese DG. Heating of magnetorheological fluid dampers. J Intell Mater Syst Struct 1999;10: 634-645.

[12] Beeby SP, Tudor MJ, White NM. Energy harvesting vibration sources for Microsystems applications. Meas Sci Technol 2006;17: R175-R195.

[13] Priya S, Inman DJ. Energy harvesting technologies. Spinger Science+Business Media, LLC;2009.

[14] Beeby SP, Tudor MJ, Torah RN, Roberts S, O'Donnell T, Roy S. Experimental comparison of macro and micro scale electromagnetic vibration powered generators. Microsystem Technol 2007; 13: 1647-1653.

[15] Anton SR, Sodano HA. A review of power harvesting using piezoelectric materials (2003–2006).Smart Mater Struct 2007; 16:R1-R21.

[16] Mitcheson PD, Miao P, Stark BH, Yeatman EM, Holmes AS, Green TC. MEMS electrostatic micro-power generator for low frequency operation. Sens Actuators A 2004; 115: 523-529.

[17] Kornbluh RD, Pelrine R, Pei Q, Heydt R, Stanford S, Oh S,Eckerle J. Electroelastomers: applications of dielectric elastomer transducers for actuation, generation, and smart structures. In: Proc. of SPIE Smart Struct. Mater. Conference ;2002. p. 254-270.
[18] Ottman GK, Hofmann HF, Bhatt AC, Lesieutre GA. Adaptive piezoelectric energy harvesting circuit for wireless sensor remote power supply.IEEE Trans on Power Electron 2002;17(5): 669-676.
[19] Lynch JP, Loh KJ.A summary review of wireless sensors and sensor networ- ks for structural health monitoring. Shock Vib Dig 2006; 38:2,91-128.
[20] Bogue R. Energy harvesting and wireless sensors: a review of recent developments. Sens Rev 2009;29(3): 194-199.
[21] Casciati F, Rossi R. A power harvester for wireless sensing applications. Struct Control Health Monit 2007;14: 649-659.
[22] Torah R, Glynne-Jones P, Tudor M, O'Donnell T, Roy S, Beeby S. (2009) Self-powered autonomous wireless sensor node using vibration energy harvesting. Meas Sci Technol 2009; 19: 125202.
[23] Sazonov E, Li H, Curry D, Pillay P. Self-powered sensors for monitoring of highway bridges. Sens J. IEEE 2009;9: 1422-1429.
[24] Miller TI, Spencer BF, Li J,Jo H. Solar energy harvesting and software enhancements for autonomous wireless smart sensor network. NSEL Report No. NSEL-022, Department of Civil and Environmental Engineering, University of Illinois at Urbana-Champaign, IL, USA,2010.
[25] Jang S, Jo H, Cho S, Mechitov K, Rice JA, Sim SH, Jung HJ, Yun CB, Spencer BF, Agha G. (2010) Structural health monitoring of a cable-stayed bridge using smart sensor technology: deployment and evaluation. Smart Struct Syst 2010; 6(5-6): 439-459.
[26] Wendel GR, Stecklein GL.A regenerative active suspension system. SAE Publication SP-861;1991.Paper No. 910659,p.129-135.
[27] Suda Y, Shiiba T. A new hybrid suspension system with active control and energy regeneration. Veh Syst Dyn Suppl 1996; 25: 641-654.
[28] Kim YB, Hwang WG, Kee CD, Yi HB. Active vibration control of a suspension system using an electromagnetic damper. In:Proc. Inst. Mech. Eng. D; 2001. 215,p. 865-873.
[29] Graves KE. Electromagnetic energy regenerative vibration damping. Ph.D. Thesis, Industrial Institute Swinburne, Swinburne University of Technology, Hawthorn, Victoria, Austria;2000.
[30] Nakano K, Suda Y, Nakadai S. Self-powered active vibration control using a single electric actuator. J Sound Vib 2003;260:2,213-235.
[31] Lesieutre GA, Ottman GK, Hofmann HF. Damping as a result of piezoelectric energy harvesting. J Sound Vib2004; 269: 991-1001
[32] Liang JR, Liao WH. Piezoelectric energy harvesting and dissipation on structural damping. J Intell Mater Syst Struct 2009; 20: 515-527.
[33] Auge LJ. Structural magnetic induction dampers in buildings. Master thesis, Department of Civil and Environmental Engineering, Massachusetts Institute of Technology, MA, USA;2003.
[34] Behrens S, Fleming AJ, Reza Moheimani SO. Passive vibration control via electromagnetic shunt damping. IEEE/ASME Trans. Mech 2005; 20: 118-122.
[35] Palomera-Arias R, Connor JJ,Ochsendorf JA. Feasibility Study of Passive Electromagnetic Damping Systems. ASCE J Struct Engng 2008;134:1, 164-170.
[36] Palomera-Arias R. Passive Electromagnetic Damping Device for Motion Control of Building Structures. PhD Dissertation. Massachusetts Institute of Technology, USA;2005.

[37] Inoue T, Ishida Y, Sumi M. Vibration suppression using electromagnetic resonant shunt damper. J Vib Acoust 2008;130(4): 041003.
[38] Niu H, Zhang X, Xie S, Wang P. A new electromagnetic shunt damping treatment and vibration control of beam structures. Smart Mater Struct 2009;18: 045009.
[39] Cheng TH, Oh IK. A current-flowing electromagnetic shunt damper for multi-mode vibration control of cantilever beams. Smart Mater Struct 2009;18: 095036.
[40] Zhang C, Ou J. Control structure interaction of electromagnetic mass damper system for structural vibration control. J Engng Mech 2008; 134(5): 428-437.
[41] Stephen NG. On energy harvesting from ambient vibration. J Sound Vib 2006;293: 409-425.
[42] Hambley AR. Electrical Engineering, Principles and Applications. Pearson Prentice Hall, Upper Saddle River, New Jersy,USA;2008.
[43] Du PA, Plitz I, Menocal S, Amatucci G. A comparative study of Li-ion battery, supercapacitor and nonaqueous asymmetric hybrid devices for automotive applications. J Power Sources 2003; 115(1):171-178.

Table 1. Optimal output power and optimal energy conversion efficiency in Case 2

| $f$ (Hz) | $d$ (mm) | Testing | | Modelling | |
|---|---|---|---|---|---|
| | | $\overline{P}_{\text{out,max}}$ (mW) | $\eta_{\text{max}}$(%) | $\overline{P}_{\text{out,max}}$ (mW) | $\eta_{\text{max}}$(%) |
| 2 | 3 | 2.5 | 14.4 | 2.5 | 13.2 |
| | 6 | 9.8 | 20.8 | 9.9 | 19.5 |
| | 11 | 30.2 | 25.9 | 33.4 | 25.2 |
| 6 | 3 | 24.9 | 23.2 | 22.3 | 23.4 |
| | 6 | 97.7 | 29.9 | 89.3 | 29.4 |
| | 11 | 274.3 | 33.1 | 300.2 | 33.3 |

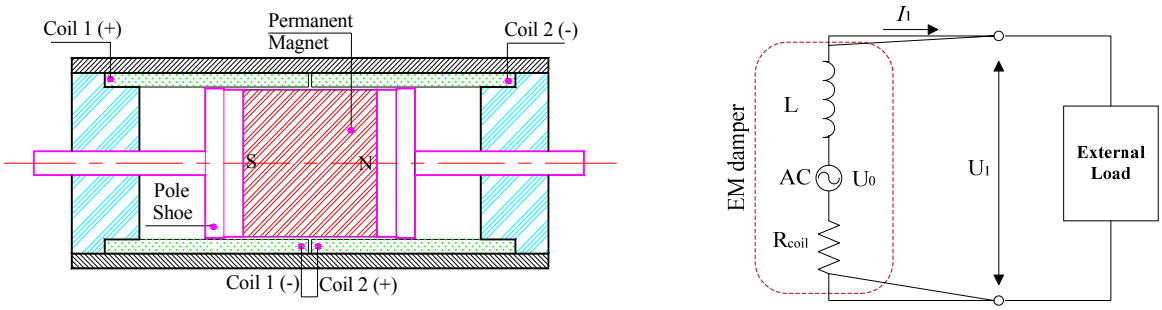


(a) Typical configuration [30] (b) Simplified model

Figure 1 Linear Moving-magnet EM Dampers

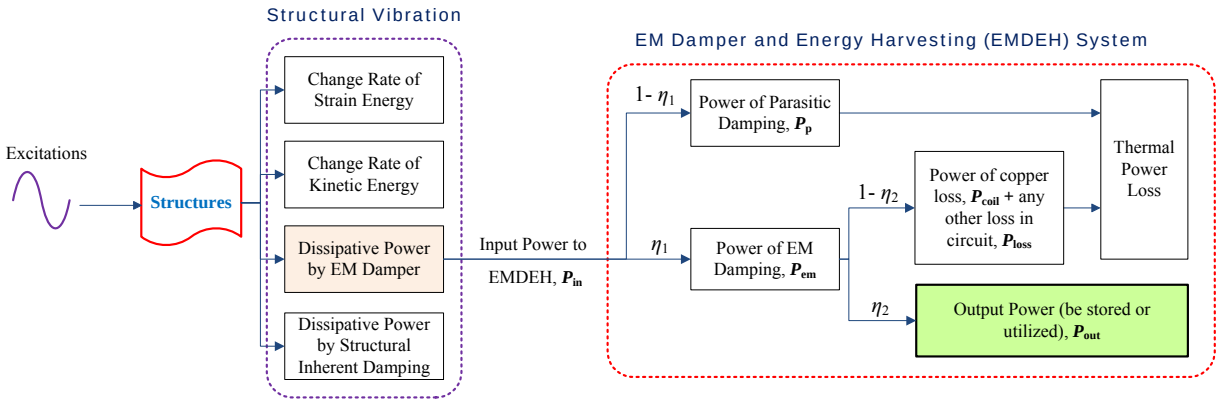


Figure 2 Power flow of a structure with an EMDEH system

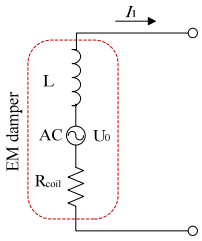


(a) Open circuit

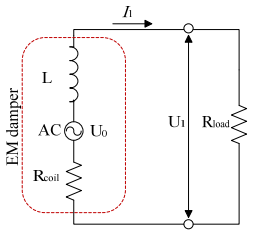


(b) Circuit with constant resistor

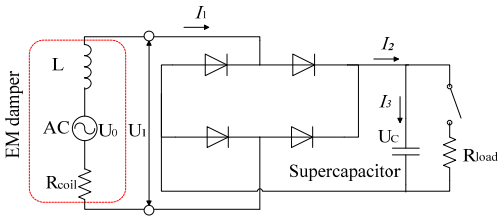


(c) Circuit with rectifier and supercapacitor

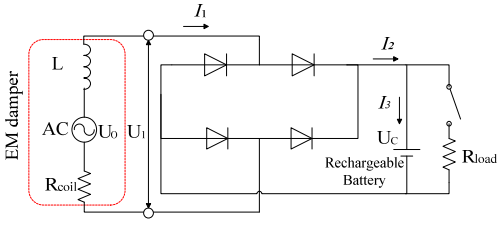


(d) Circuit with rectifier and rechargeable battery

Figure 3. EM damper connected with four different circuits

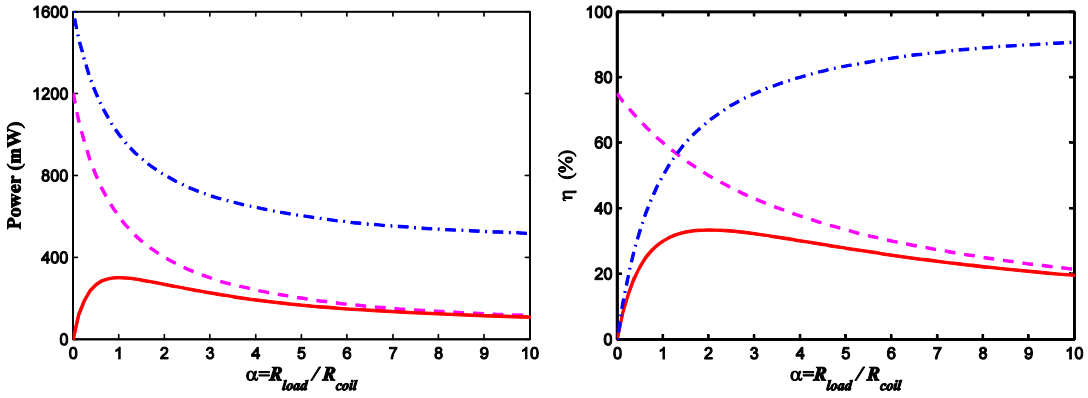


(a) power (b) energy conversion ratios

Figure 4. Theoretical variation of power and energy conversion efficiency of EMDEH system with parameter $\alpha$ in Case 2

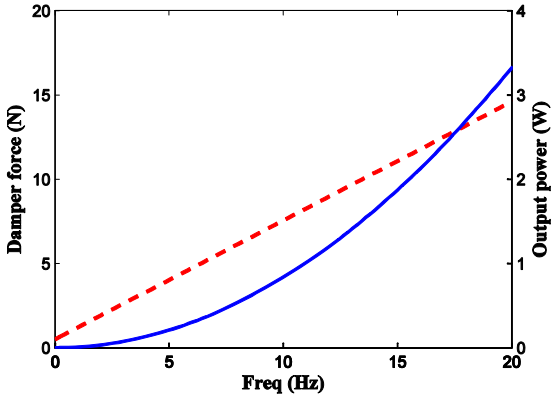


Figure 5. Theoretical variation of peak damper force and output power with frequency in Case 2 (d=11mm, $R_{load}$=4Ω)

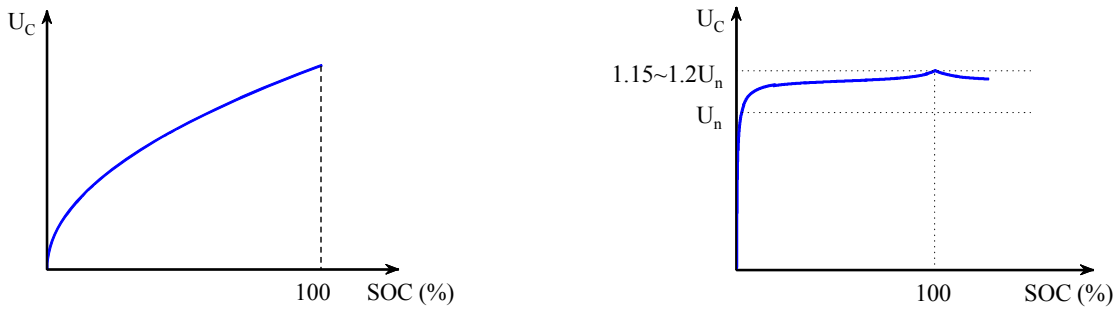


(a) supercapacitor (b) NiHM rechargeable battery

Figure 6. Typical charge characteristics of supercapacitor and NiHM battery (SOC: State-of-Charge)

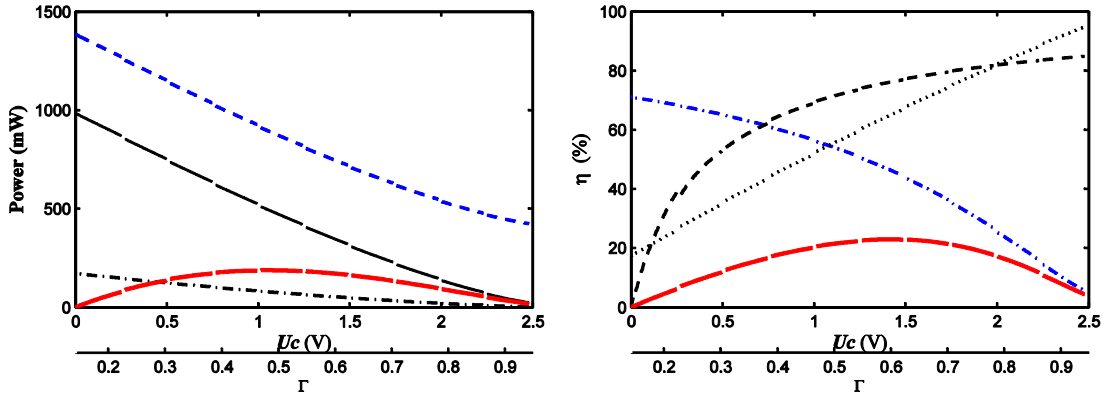


(a) power (b) energy conversion ratios

Figure 7. Theoretical variation of power and energy conversion efficiency of EMDEH system with parameter Γ (or $U_C$) in Case 3

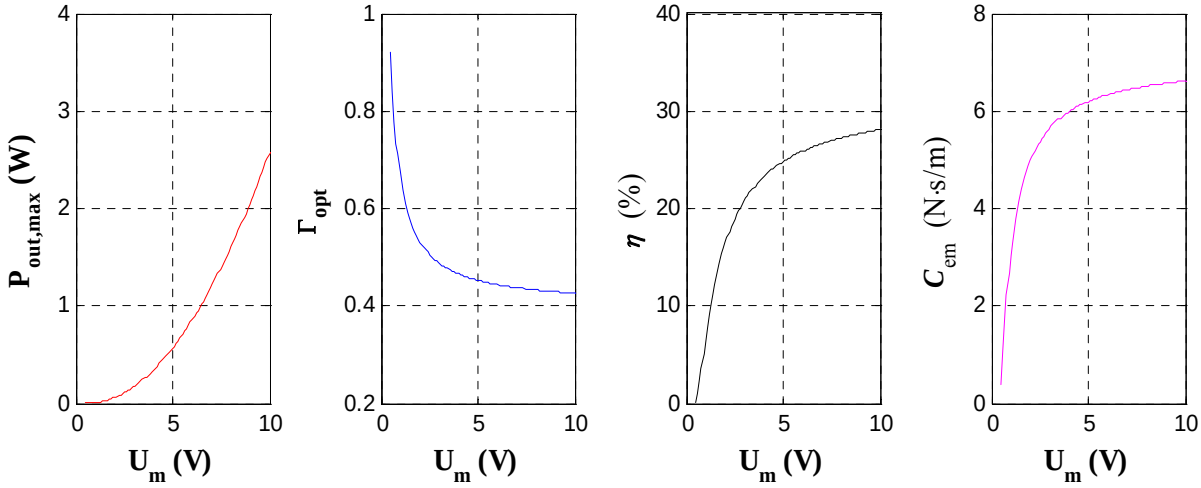


Figure 8: The variation of maximum output power and other corresponding quantities with the increasing $U_m$ in Case 3

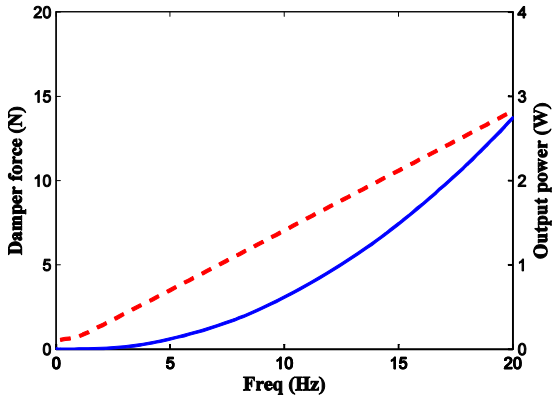


Figure 9. The variation of peak damper force and optimal output power with excitation frequency in Case 3 (d=11mm, $\Gamma_{opt} = 0.4 + 1.2 V_F / U_m$ )

(a) EM damper tested on MTS machine

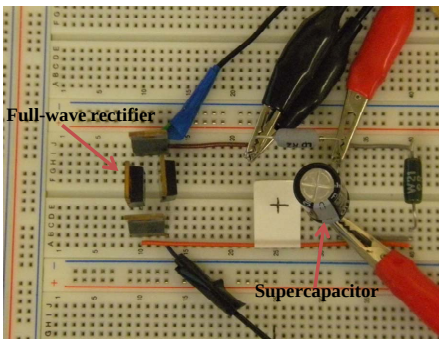


(b) circuit in Case 3

Figure 10. Experimental setup

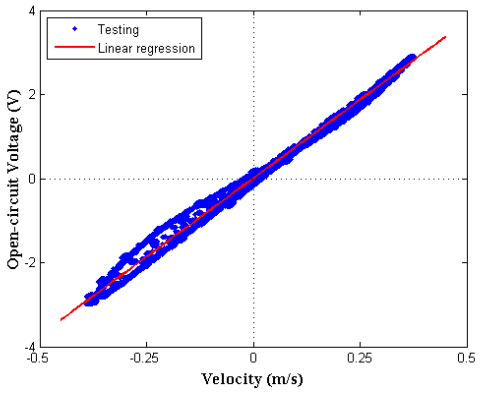


Figure 11. Open circuit voltage vs. velocity relation

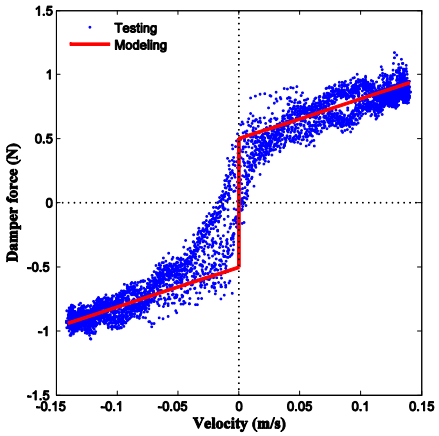


Figure 12. Damper force vs. velocity relationship in Case 1 ($f$ = 2Hz, $d$ = 11mm)

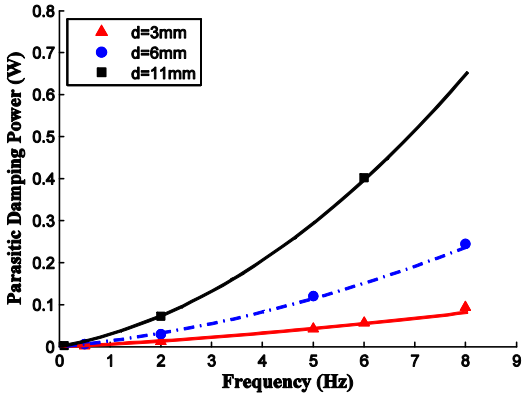


Figure 13. Parasitic damping powers in Case 1(Line: Modeling by Equation (5); Dots: Testing)

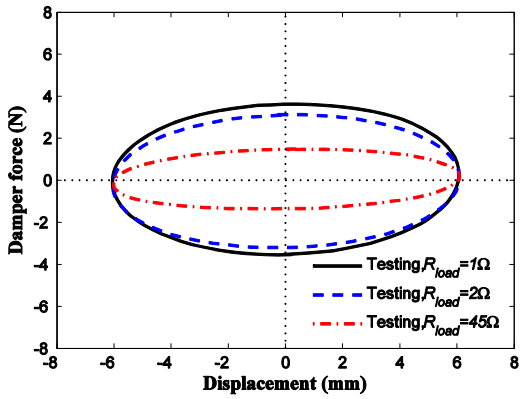


Figure 14. The effect of $R_{load}$ on force-displacement behavior in Case 2 ($f$ = 6 Hz, $d$ = 6 mm)

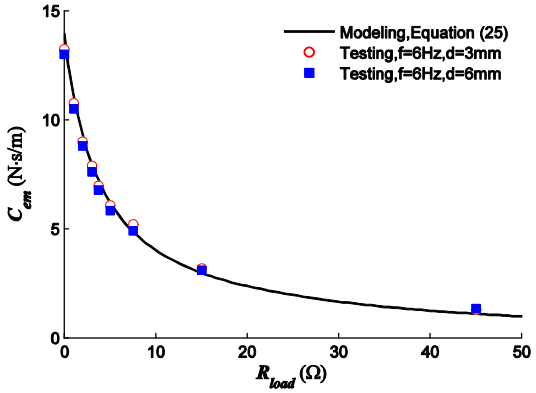


Figure 15. The relation of EM damping coefficient $C_{em}$ vs. load resistance $R_{load}$ in Case 2

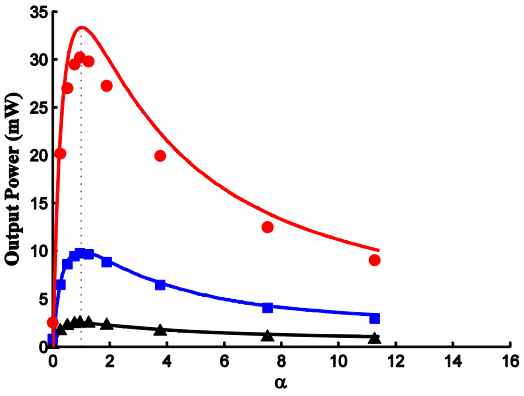


(a) $f$=2Hz

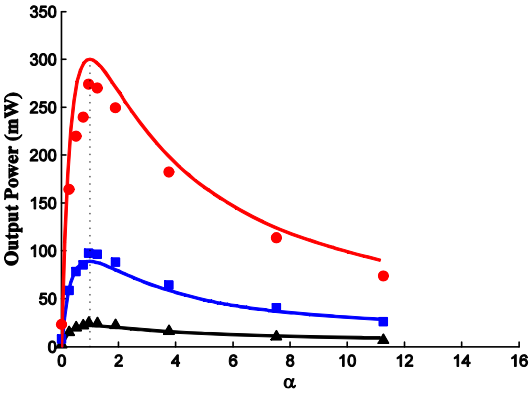


(b) $f$=6Hz

Figure 16. The relations of output power $\overline{P}_{\text{out}}$ vs. α in case 2

(Line: Modeling by Equation (30); Dots: Testing)

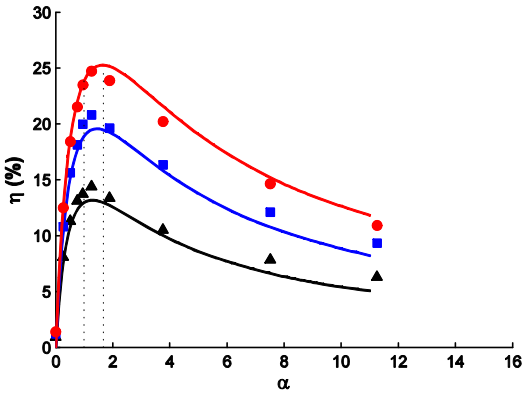


(b) $f$=2Hz

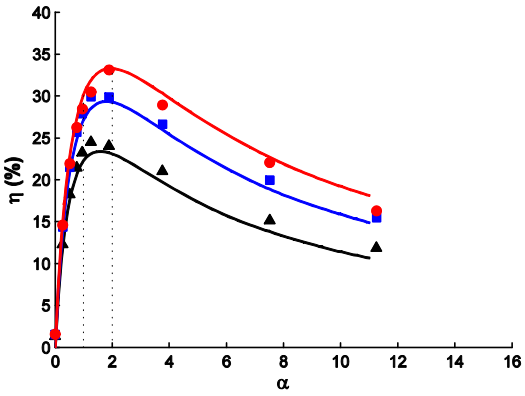


(b) $f$=6Hz

Figure 17. Energy conversion efficiency vs. α in Case 2

(Line: Modeling by Equation (33); Dots: Testing)

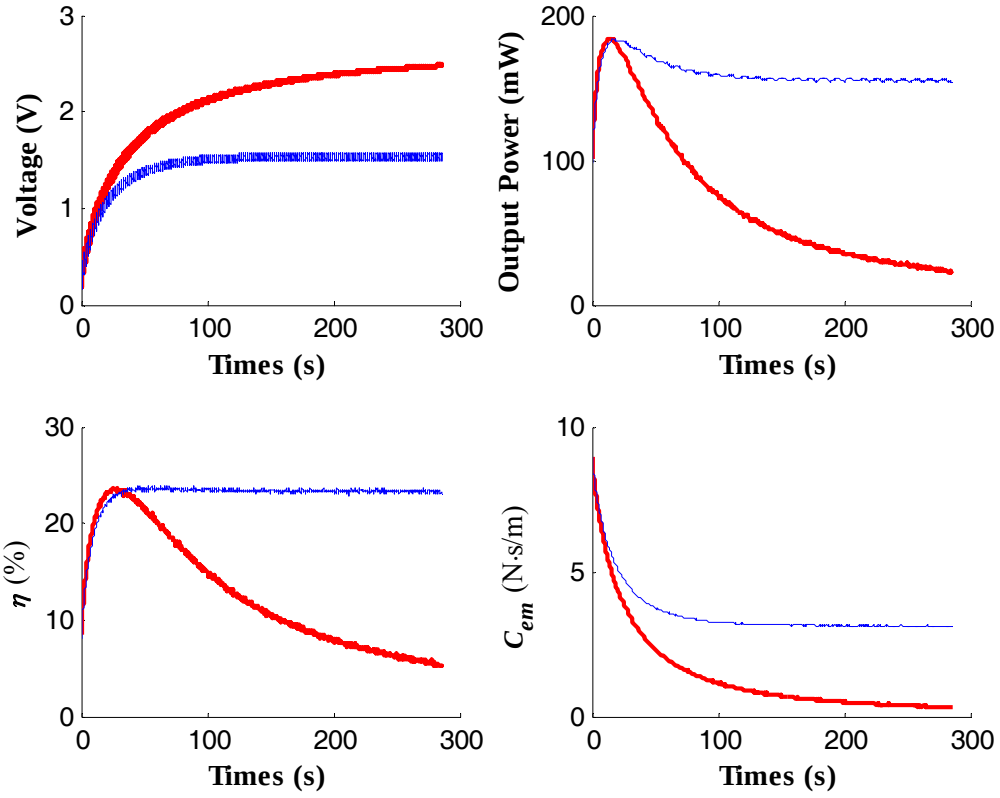


Figure 18. Time histories of supercapacitor voltage $U_C$, EM damping $C_{em}$, output power $\overline{P}_{out}$ and energy conversion efficiency η in Case 3 ($f$ = 6Hz, $d$ = 11mm, Curve I: Switch open, Curve II: $R_{load}$=15Ω)

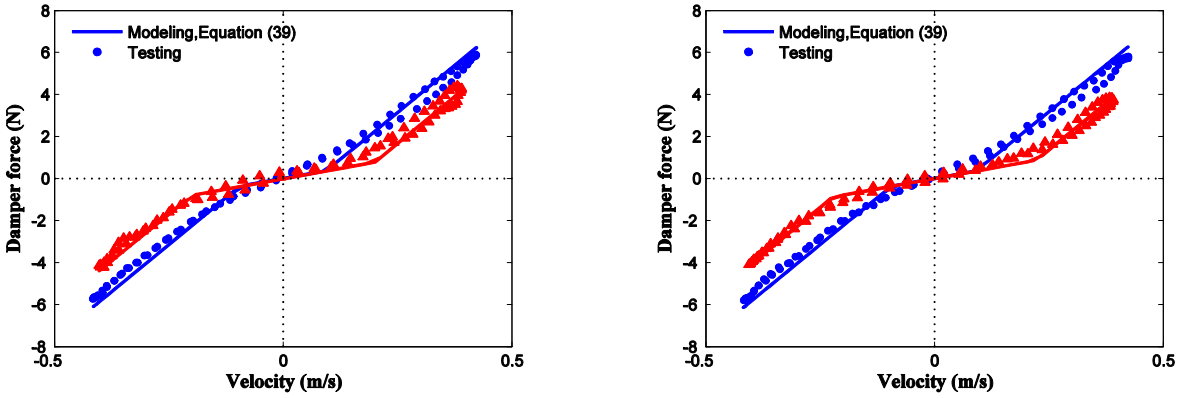


(a) Switch open (b) $R_{load}$=15Ω

Figure 19. Damper force vs. velocity in Case 3 ($f$ = 6Hz, $d$ = 11mm)

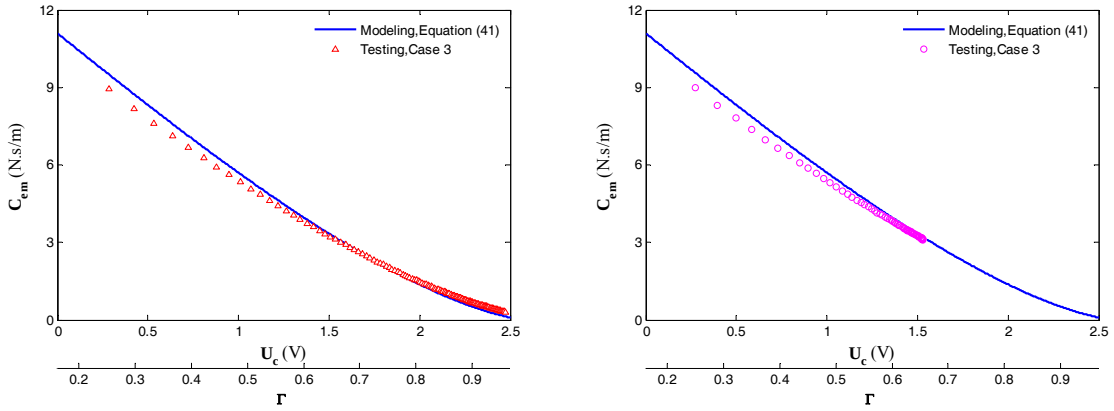


(a) Switch open (b) $R_{load}$=15Ω

Figure 20. EM Damping coefficients in charging process in Case 3 ($f$ = 6Hz, $d$ = 11mm)

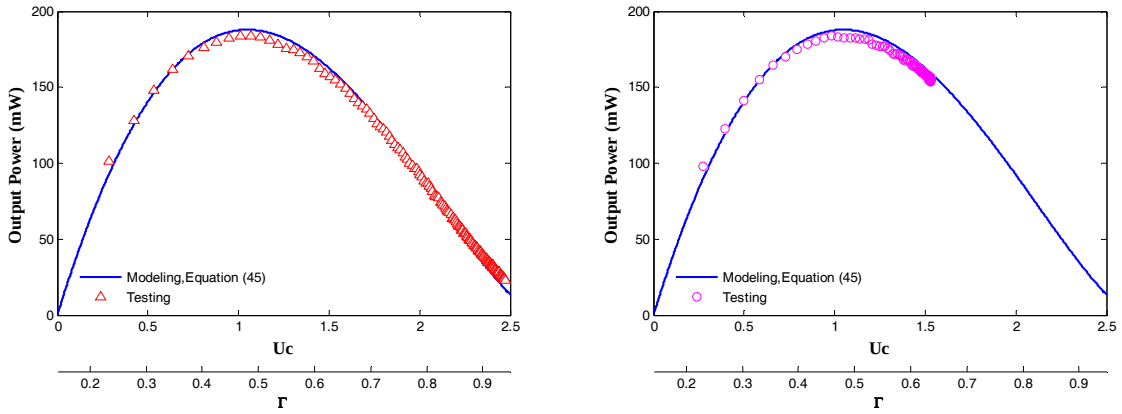


(a) Switch open (b) $R_{load}$=15Ω

Figure 21. Output power $\overline{P}_{out}$ in charging process in Case 3 ($f$ = 6Hz, $d$ =11mm)

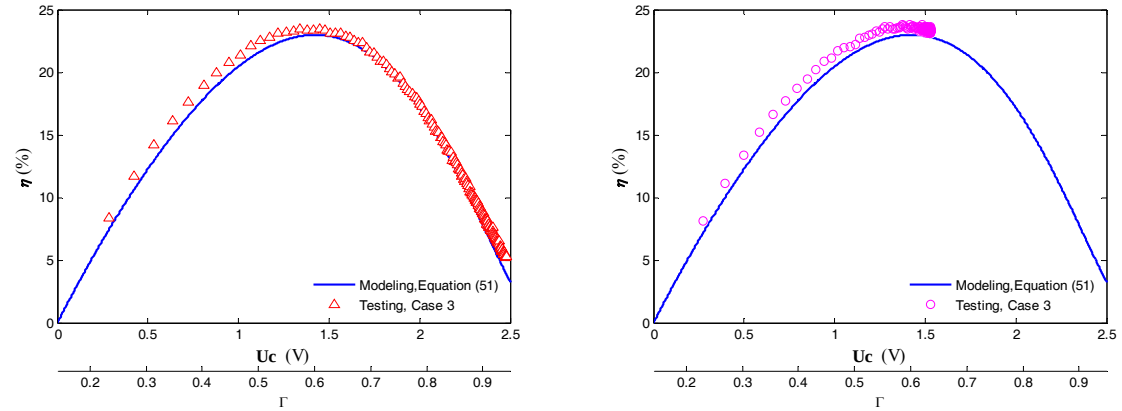


(a) Switch open (b) $R_{load}$=15Ω

Figure 22. Energy conversion efficiency η in charging process in Case 3 ($f$ =6Hz, $d$ =11mm)

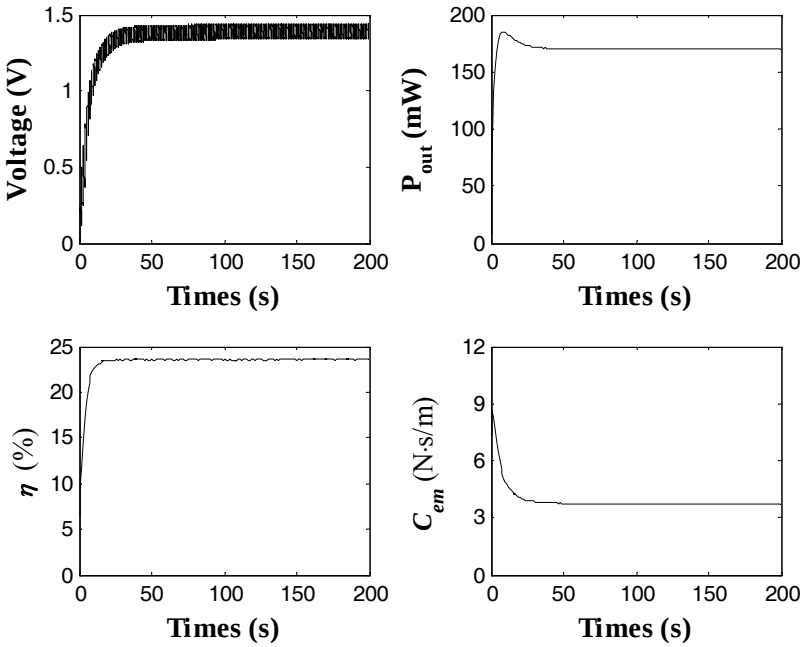


Figure 23. Time histories of battery voltage $U_C$, EM damping $C_{em}$, output power $\overline{P}_{out}$ and energy conversion efficiency η in Case 4 ($f$ = 6Hz, $d$ = 11mm, $R_{load}$ = 15Ω)